AN ENHANCEMENT OF KRIGING BASED FINITE ELEMENT FOR PLATE ANALYSIS BY USING MITC3+ ELEMENT

Sebastian[1], F.T. Wong[2]
[1] Department of Civil Engineering, Petra Christian University, Jalan Siwalankerto 121-131, Surabaya 60236, Indonesia

[1] b21200003@john.petra.ac.id, [2] wftjong@petra.ac.id

ABSTRACT: A development of Kriging-based finite elements method has been carried out by implementing the MITC3+ plate elements for modeling the plate structure. The MITC3+ element used is a development of the MITC3 element whose performance is considered quite good and can overcome problems that arise in the application of conventional Kriging-based finite elements, one of which is the shear-locking. The application of Kriging interpolation on MITC3+ elements is carried out with the Kriging shape function formulation in the formation of the bending stiffness matrix only. The elements are then tested with various benchmark problems such as *Patch Test*, hard clamped square plate*, Rhombic Plate*, and its ability to solve complex-shaped plates. The results showed that the MITC3+ was able to avoid the shear-locking mechanism and also produce an accurate solution. However, it appears there is an inconsistent convergence pattern on the *Patch Test* and *Rhombic Plate*.

Keywords: *plate structure, finite element method*, *kriging interpolation*, *MITC3+ element*, *shear-locking*

1. INTRODUCTION

The finite element method (FEM) is a popular numerical approach used for analyzing plate bending structures (I. Katili et al., 2019; Nguyen-Xuan et al., 2010; Verwoerd & Kok, 1990). In early development, Kirchhoff plate theory was used as the basic structural modeling for analysis which neglects the shear deformation behavior in the plate structure. Hereafter, the theory began to shift into a more general and accurate plate theory that considers the shear deformation behavior, known as the Reissner-Mindlin theory (RM). However, the use of the conventional FEM for modeling the RM element still suffers from the shear-locking phenomenon. Many research has been done in attempts to alleviate this severe problem that causes the element to become too stiff in a pure bending situation, but the shear-locking cannot be eliminated in a certain condition where the mesh is distorted (P. S. Lee et al., 2007; Y. Lee et al., 2012).

In contrast to the conventional FEM approach, the Kriging-based FEM (K-FEM) proposed by Plengkhom & Kanok-Nukulchai (Plengkhom & Kanok-Nukulchai, 2005) uses a set of data obtained from various *nodes* around the domain of influence (DOI) composed in several layers of elements. This approach allows the solution to be obtained more accurately and has a smoother field of displacement while still maintain the simplicity of the element, mainly the triangular element used in this paper. Further research by Wong & Kanok-Nukulchai (Wong & Kanok-Nukulchai, 2009) pointed that this approach has *non-conforming* behavior. To overcome the locking phenomenon, Wijaya (Wijaya, 2016) has proposed the application of

the discrete shear gap (DSG) method and Wong & Kanok-Nukulchai (Wong & Kanok-Nukulchai, 2006) with the assumed natural strain (ANS) method in K-FEM. However, the locking persists due to the inadequate determination of shear strain sampling.
Another promising approach is to incorporate a better performance element of a triangular RM plate into K-FEM to deal with the shear-locking. The element based on ANS was proven to be great at the reduction of shear-locking, with the name of T3γ (Tessler & Hughes, 1985). It also appears to have the same element stiffness matrix as the mixed interpolation of tension component (MITC) based element called MITC3 (P. S. Lee & Bathe, 2004) with a slightly different way to obtain (A. M. Katili et al., 2019a). Recently, MITC3 has been developed into a better performing element called MITC3+ (Jeon et al., 2015) with the addition of a cubic *bubble function* to enhance the approximation of the rotation field inside the element and the new assumed natural shear strain field.
This present paper aims to examine the performance of K-FEM with the MITC3+ element with the hope of delivering a better performing, shear-locking free element by incorporating that two methods.

2. KRIGING INTERPOLATION

In the first place, KI was used as a geostatic method in mining to get data from one random point by interpolating another data from various data points in the space. K-FEM is a development of conventional FEM that works on a matrix system with the concept *direct stiffness method* with the addition of its Kriging interpolation (KI) schemes. It's also has been applied for generating a new Kriging-based shape function that obtained from the interpolation of not only one element, but other elements inside the domain of influence (DOI). A more detailed explanation and derivation of the Kriging interpolation may be found in literature from (Tongsuk & Kanok-Nukulchai, 2004).
Formulation starts by considering a continuous field variable $u(\boldsymbol{x})$ defined in a domain Ω. For a random *nodes* $\boldsymbol{x}_0$, the value of $u(\boldsymbol{x}_0)$ is assumed to be influenced by its surrounding *nodes* inside a subdomain (DOI), and then it can be calculated using the estimated value of u^h which is a linear combination in the form,

$$u^h(\boldsymbol{x}_0) = \sum_{i=1}^{n} \lambda_i u(\boldsymbol{x}_i) \tag{1}$$

where λ_i is the Kriging weights for each *nodes* inside DOI, and *n* is the number of node inside DOI. In KI, the deterministic function of $u(\boldsymbol{x})$ can be considered as the realization of the random function of $U(\boldsymbol{x})$, so it can be written as follows,

$$U^{\mathrm{h}}(\mathbf{x}_0) = \sum_{i=1}^{n} \lambda_i U(\mathbf{x}_i) \tag{2}$$

The Kriging weights are determined on the condition that the estimated value $U^{\mathrm{h}}(\mathbf{x}_0)$ is unbiased, and so it was written as follows,

$$\mathrm{E}[U^{\mathrm{h}}(\mathbf{x}_0) - U(\mathbf{x}_0)] = 0 \tag{3}$$

Apart from being unbiased, the variances of estimation error must also be minimized using $\mathrm{var}[U^{\mathrm{h}}(\mathbf{x}_0) - U(\mathbf{x}_0)] = 0$. Using the Lagrange multiplier method, a system of Kriging equations can be formulated. The derivation of the complete and clear formulation of the Kriging equation

can be seen in research by Wong & Kanok-Nukulchai (2009) and Wijaya (2016). The formulation is as follows,

$$\mathbf{R\lambda} + \mathbf{P\mu} = \mathbf{r}(\mathbf{x_0}) \quad (4)$$

$$\mathbf{P}^{\mathrm{T}}\boldsymbol{\lambda} = \mathbf{p}(\mathbf{x_0}) \quad (5)$$

with,

$$\mathbf{R} = \begin{bmatrix} C(\mathbf{h}_{11}) & \dots & C(\mathbf{h}_{1n}) \\ \dots & \dots & \dots \\ C(\mathbf{h}_{n1}) & \dots & C(\mathbf{h}_{nn}) \end{bmatrix} \quad (6)$$

$$\mathbf{P} = \begin{bmatrix} p_1(\mathbf{x}_1) & \dots & p_m(\mathbf{x}_1) \\ \dots & \dots & \dots \\ p_1(\mathbf{x}_n) & \dots & p_m(\mathbf{x}_n) \end{bmatrix} \quad (7)$$

$$\boldsymbol{\lambda} = [\lambda_1 \quad \dots \quad \lambda_n]^T, \ \boldsymbol{\mu} = [\mu_1 \quad \dots \quad \mu_m]^T \quad (8)$$

$$\mathbf{r}(\mathbf{x}_0) = [C(\mathbf{h}_{10}) \quad \dots \quad C(\mathbf{h}_{n0})]^T, \ \mathbf{p}(\mathbf{x}_0) = [p_1(\mathbf{x}_0) \quad \dots \quad p_m(\mathbf{x}_0)]^T \quad (9)$$

where **R** is the covariance matrix $C(\mathbf{h}_{ij})$, **P** is an n × m matrix of polynomial values at the *nodes*, **λ** is a vector of Kriging weights, **μ** is a vector of Lagrange multipliers, $\mathbf{r}(\mathbf{x_0})$ is a vector of covariance between the *nodes* and the node of interest, $\mathbf{x_0}$, and $\mathbf{p}(\mathbf{x_0})$ is a vector of polynomial basis at $\mathbf{x_0}$.

Meanwhile, because **λ** is a vector with the dimension of *n* × 1, equation (2.1) can be written as,

$$u(\mathbf{x}_0) = \boldsymbol{\lambda}^{\mathrm{T}}\mathbf{d} \quad (10)$$

where $\mathbf{d} = [u(\mathbf{x}_1) \quad \dots \quad u(\mathbf{x}_n)]^{\mathrm{T}}$ is a vector from *nodes*. By using FEM expressions, that equation can resemble the relation equation between *shape function* and nodal displacement which can be expressed as,

$$u^{\mathrm{h}}(\mathbf{x}) = \mathbf{N}(\mathbf{x})\mathbf{d} = \sum_{i=1}^{n} N_i(\mathbf{x})u_i \quad (11)$$

where $\mathbf{N}(\mathbf{x}) = \boldsymbol{\lambda}^{\mathrm{T}}(\mathbf{x})$ is the Kriging *shape function*.

In K-FEM, for each element, the Kriging shape function is constructed based on a set of *nodes* in a predetermined DOI which has several layers of element. The number of layers for standard FEM is only one, which includes only the element itself. Whereas in K-FEM, the DOI is determined according to needs, and of course the more DOI's are reviewed, the more accurate the results will be, but the duration for the work to be done also longer.

Polynomial bases that play a role in the formation of the Kriging shape functions are basic polynomial-forming functions. The table for the minimum number of DOI layers based on the polynomial basis can be seen in Table 1.

Table 1. The Minimum Number Of DOI Layers Based On The Polynomial Basis

Polynomial Basis	**Minimum number of layers**
Linear	1
Quadratic	2
Cubic	3
Quartic	4

Constructing the Kriging shape function requires a model of correlation coefficient with its function parameters. The correlation function is as follows,

$$\rho(\mathbf{h}) = C(\mathbf{h})/\sigma^2 \tag{12}$$
$$\sigma^2 = \mathrm{var}[\boldsymbol{U}(\mathbf{x})] \tag{13}$$

According to previous related research (Gu, 2003; Plengkhom & Kanok-Nukulchai, 2005; Tongsuk & Kanok-Nukulchai, 2004), σ^2 does not effect on the final results and so in this research it is taken as 1. In K-FEM there is 2 kind of correlation function, which is Gaussian with the function as follows,

$$\rho(h) = e^{-\left(\theta\frac{h}{d}\right)^2} \tag{14}$$

and the quartic spline function as follows,

$$\rho(h) = \begin{cases} 1 - 6\left(\theta\frac{h}{d}\right)^2 + 8\left(\theta\frac{h}{d}\right)^3 - 3\left(\theta\frac{h}{d}\right)^4 : \text{untuk } 0 < \theta\frac{h}{d} < 1 \\ 0 \ : \text{untuk } \theta\frac{h}{d} > 1 \end{cases} \tag{15}$$

where $\theta > 0$ is the correlation parameter, h is the distance of two nodal points, and d is the maximum distance between pairs of nodal points on the DOI. According to Plengkhom & Kanok-Nukulchai (2005), the correlation parameters should be selected so that it satisfies the lower bound,

$$\left|\sum_{i=1}^{n} N_i - 1\right| \leq 1 \times 10^{-10+a} \tag{16}$$

and the upper bound,

$$\det(\mathbf{R}) \leq 1 \times 10^{-b} \tag{17}$$

with a is the order of basis function (for *linear*, a = 1; *quadratic*, a = 2; *cubic*, a = 3, *quartic*, a = 4; and b is the dimension of the problem (1, 2, or 3).

3. KRIGING-BASED MITC3+ FORMULATION

The present research with K-FEM used the MITC3+ (I. Katili et al., 2019) as the element modeling base. The MITC3+ element was initially modeled in term of shell element (Jeon et al., 2015), but it has been modeled as a plate in a slightly different manner (I. Katili et al., 2019) with the original version of MITC3+ (Jeon et al., 2015; Ko et al., 2017), with changes in notation and differences of the *bubble function* formulation located in the center of the element to increase the rotation *dof* (*degree of freedom*) and also the different assumption of transverse strain fields for the *tying points*. With the addition of the *cubic bubble function* (P_7) for the center node of the element, the displacement and rotation of the MITC3+ element equipped with the Kriging interpolation is defined in a form of,

$$w = \sum_{i=1}^{n} N_i w_i \tag{18}$$
$$\beta_x = \sum_{i=1}^{n} N_i \beta_{xi} + P_7 \Delta\beta_{x7} \tag{19}$$

$$\beta_y = \sum_{i=1}^{n} N_i \beta_{yi} + P_7 \Delta\beta_{y7} \quad (20)$$

where P_7 is the cubic function $27A_1A_2A_3$ and $\Delta\beta_{x7}$ is the normal rotation components for the additional node at the centroid. A_i that create the cubic function is the linear shape function for a triangular element which can be described as $A_1 = 1 - \xi - \eta$, $A_2 = \xi$, and $A_3 = \eta$ with respect of the element local coordinates. The distinction is located on the shape function used for the displacement at corner *nodes* of the element (N_i), none other than the Kriging shape function. With *n* is the number of *nodes* inside DOI.

Now for the formulation, consider a homogeneous plate with uniform thickness in a three-dimensional Cartesian coordinate system with the *x-y* plane is on the middle surface of the plate. The rotation of a normal line has two components, namely β_x and β_y. The positive sign for these rotation components and displacement components is shown in Figure 1.

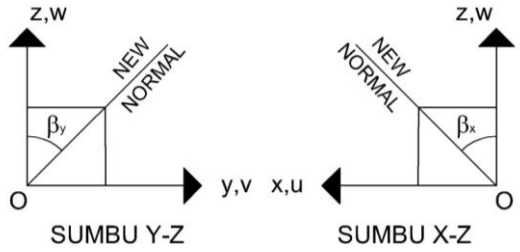

Figure 1. The Positive Sign For The Displacement And Rotation Components
Source: (I. Katili, 1993)

The displacement field then can be described by,

$$u = z\,\beta_x(x,y) \quad (21)$$
$$v = z\,\beta_y(x,y) \quad (22)$$
$$w = w\,(x,y) \quad (23)$$

where *w* is the vertical deflection in the *z*-direction and β_x, β_y are the normal line rotational component around its midpoint. The governing equation is formed by the principle of virtual displacement of the Reissner-mindlin plate as follows,

$$\int_V \delta\boldsymbol{\varepsilon}_{\mathrm{b}}{}^{\mathrm{T}}\boldsymbol{\sigma}_{\mathrm{b}}\,dV + \int_V \delta\boldsymbol{\varepsilon}_{\mathrm{s}}{}^{\mathrm{T}}\boldsymbol{\sigma}_{\mathrm{s}}\,dV = \int_S \delta w^{\mathrm{T}} q\,dS \quad (24)$$

where $\boldsymbol{\delta\varepsilon}_{\mathrm{b}}$ is the virtual bending strain, $\boldsymbol{\delta\varepsilon}_{\mathrm{s}}$ is the virtual shear strain and $\boldsymbol{\delta w}$ is the virtual deflection. The equation and then can be also described with the weak form as,

$$\int_S \delta\boldsymbol{\kappa}^{\mathrm{T}}\mathbf{D}_{\mathrm{b}}\boldsymbol{\kappa}\,dS + \int_S \delta\boldsymbol{\varepsilon}_{\mathrm{s}}{}^{\mathrm{T}}\mathbf{D}_{\mathrm{s}}\boldsymbol{\varepsilon}_{\mathrm{s}}\,dS = \int_S \delta\mathbf{u}^{\mathrm{T}}\mathbf{p}\,dS \quad (25)$$
$$\mathbf{p} = \{q \quad 0 \quad 0\}^{\mathrm{T}} \quad (26)$$

p is the surface force vector, and

$$\mathbf{D}_{\mathrm{b}} = \frac{Et^3}{12(1-v^2)}\begin{bmatrix} 1 & v & 0 \\ v & 1 & 0 \\ 0 & 0 & \frac{(1-v)}{2} \end{bmatrix} = D_b \begin{bmatrix} 1 & v & 0 \\ v & 1 & 0 \\ 0 & 0 & \frac{(1-v)}{2} \end{bmatrix} \quad (27)$$

for the elasticity matrix for bending deformation, and

$$\mathbf{D}_{\mathrm{s}} = Gkt\begin{bmatrix}1 & 0\\ 0 & 1\end{bmatrix} = D_s\begin{bmatrix}1 & 0\\ 0 & 1\end{bmatrix} \tag{28}$$

is the elasticity matrix for transverse shear deformation, with *G = E 2(1 + v)* as the shear modulus, and *k* is the shear correction factor taken as *5/6* for homogeneous. *E* is the material property of *Young's modulus*, and *v* is the *Poisson's ratio.*

Like the explanation before, the key of application of the Kriging Interpolation into FEM is the new Kriging-based shape function that is used to obtain the approximate solution. Suppose the DOI is subdivided by the number of *n nodes*. Then the element field of displacement can be written in matrix as follows,

$$\begin{Bmatrix}w\\ \beta_x\\ \beta_y\end{Bmatrix} = \sum_{i=1}^{n}\begin{bmatrix}N_i & 0 & 0\\ 0 & N_i & 0\\ 0 & 0 & N_i\end{bmatrix}\begin{Bmatrix}w_i\\ \beta_{xi}\\ \beta_{yi}\end{Bmatrix} + 27A_1A_2A_3\begin{Bmatrix}0\\ \Delta\beta_{x7}\\ \Delta\beta_{y7}\end{Bmatrix} \tag{29}$$

The curvatures then can be expressed as,

$$\boldsymbol{\kappa} = \begin{Bmatrix}\beta_{x,x}\\ \beta_{y,y}\\ \beta_{x,y} + \beta_{y,x}\end{Bmatrix} \tag{30}$$

$$\boldsymbol{\kappa} = \mathbf{B_{b\beta}}\,\mathbf{d} + \mathbf{B_{b\Delta\beta}}\,\Delta\boldsymbol{\beta}_{\mathbf{n}} \tag{31}$$

with $\mathbf{d} = \{w_1\ \beta_{x1}\ \beta_{y1}\ w_2\ \beta_{x2}\ \beta_{y2}\ w_3\ \beta_{x3}\ \beta_{y3}\}^T$ is the corner *nodes* displacement and rotation and $\Delta\boldsymbol{\beta}_{\mathbf{n}} = \{\Delta\beta_{x7}\ \Delta\beta_{y7}\}^T$ is the increment centroid node rotation.

The $\mathbf{B_{b\beta}}$ is the same bending stiffness matrix as $\mathbf{B}_{\mathrm{b}}$ from the formulation of K-FEM which is,

$$\mathbf{B}_{\mathrm{b}} = \begin{bmatrix}0 & N_{1,x} & 0 & \dots & 0 & N_{n,x} & 0\\ 0 & 0 & N_{1,y} & \dots & 0 & 0 & N_{n,y}\\ 0 & N_{1,y} & N_{1,x} & \dots & 0 & N_{n,y} & N_{n,x}\end{bmatrix} \tag{32}$$

And as for $\mathbf{B_{b\Delta\beta}}$ in the matrix form,

$$\mathbf{B_{b\Delta\beta}} = \begin{bmatrix}P_{7,x} & 0\\ 0 & P_{7,y}\\ P_{7,y} & P_{7,x}\end{bmatrix} \tag{33}$$

$$P_{7,x} = j_{11}P_{7,\xi} + j_{12}P_{7,\eta}\ ;\ P_{7,y} = j_{21}P_{7,\xi} + j_{22}P_{7,\eta} \tag{34}$$

For $\mathbf{j}$ is the inverse of *jacobian* $\mathbf{J}$ consisting of j_{11}, j_{12}, j_{21}, j_{22}, the relation can be expressed as,

$$\mathbf{J} = \begin{bmatrix}x_{,\xi} & y_{,\xi}\\ x_{,\eta} & y_{,\eta}\end{bmatrix} = \begin{bmatrix}J_{11} & J_{12}\\ J_{21} & J_{22}\end{bmatrix} = \begin{bmatrix}x_{21} & y_{21}\\ -x_{13} & -y_{13}\end{bmatrix} \tag{35}$$

$$\mathbf{j} = \mathbf{J}^{-1} = \begin{bmatrix}\xi_{,x} & \eta_{,x}\\ \xi_{,y} & \eta_{,y}\end{bmatrix} = \frac{1}{det\ J}\begin{bmatrix}-y_{13} & -y_{21}\\ x_{13} & x_{21}\end{bmatrix} \tag{36}$$

$$det\,J = x_{13}y_{21} - x_{21}y_{13} \tag{37}$$

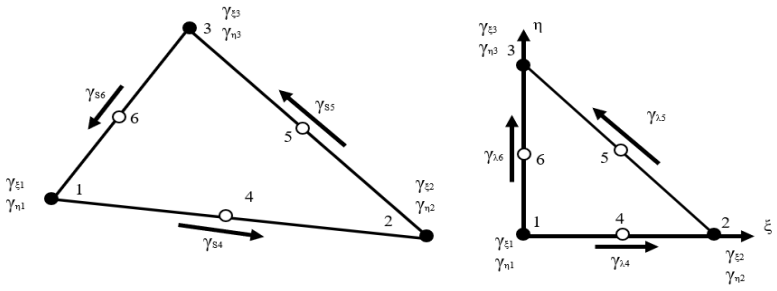

Figure 2. The Constant Shear Strain along the Edge of Element in Their Tangential Coordinate and Natural Coordinate
Source: (I. Katili et al., 2019)

Because how the *transverse shear* (TS) field of MITC3 was built, in a particular way using the local coordinate of only three main *nodes* (see Figure 2), this current research does not equip the TS field with the Kriging shape function which uses every node inside the element DOI. Therefore the assumed TS field can be obtained from the three main *nodes,* written as follows,

$$\boldsymbol{\gamma} = \begin{Bmatrix} \gamma_\xi \\ \gamma_\eta \end{Bmatrix} = \mathbf{B}^{\boldsymbol{\xi}}_{\mathbf{s\beta}_{\mathrm{MITC3+}}} \mathbf{d} + \mathbf{B}^{\boldsymbol{\xi}}_{\mathbf{s\Delta\beta}_{\mathrm{MITC3+}}} \boldsymbol{\Delta\beta_\eta} \tag{38}$$

Like previously mentioned, the addition of the TS field matrix is written as $\mathbf{B}^{\boldsymbol{\xi}}_{\mathbf{s\beta}_+}$ in the MITC3+ shear stiffness equation,

$$\mathbf{B}^{\boldsymbol{\xi}}_{\mathbf{s\beta}_{\mathrm{MITC3+}}} = \mathbf{B}^{\boldsymbol{\xi}}_{\mathbf{s\beta}_{\mathrm{MITC3}}} + \mathbf{B}^{\boldsymbol{\xi}}_{\mathbf{s\beta}_+} \tag{39}$$

The $\mathbf{B}^{\boldsymbol{\xi}}_{\mathbf{s\beta}_{\mathrm{MITC3}}}$ is the TS field matrix used in the MITC3 element that turns out to be the same as the T3γ element (A. M. Katili et al., 2019a). That TS field matrix can be constructed by linearly interpolating the strain field values at the three main *nodes* like the following equation,

$$\begin{Bmatrix} \gamma_\xi \\ \gamma_\eta \end{Bmatrix} = \sum_{i=1}^{3} A_i \begin{Bmatrix} \gamma_{\xi_i} \\ \gamma_{\eta_i} \end{Bmatrix} \tag{40}$$

or can be in the form of matrix of,

$$\begin{Bmatrix} \gamma_\xi \\ \gamma_\eta \end{Bmatrix} = \boldsymbol{A}\, \boldsymbol{\gamma_i} \tag{41}$$

$$\boldsymbol{A} = \begin{bmatrix} A_1 & 0 & A_2 & 0 & A_3 & 0 \\ 0 & A_1 & 0 & A_2 & 0 & A_3 \end{bmatrix} \tag{42}$$

where $\boldsymbol{\gamma_i} = [\gamma_{\xi 1} \quad \gamma_{\eta 1} \quad \gamma_{\xi 2} \quad \gamma_{\eta 2} \quad \gamma_{\xi 3} \quad \gamma_{\eta 3}]^T$ is the natural shear strain at node 1, 2, 3 which is obtained from the addition of constant natural shear strain throughout the edge of the element or simply called tying point 4, 5, 6 (Figure 2). The shear strain $\gamma_{\lambda k}$ and γ_{sk} are expressed in terms of the natural coordinate system and Cartesian coordinate system. Firstly, the relation between the natural shear strain at the corner *node* and the natural tying point can be written as follows,

$$\begin{Bmatrix}\gamma_{\xi_i}\\ \gamma_{\eta_i}\end{Bmatrix} = \boldsymbol{S}\begin{Bmatrix}\gamma_{\lambda_4}\\ \gamma_{\lambda_5}\\ \gamma_{\lambda_6}\end{Bmatrix} \tag{43}$$

$$\mathbf{S} = \begin{bmatrix}1 & 0 & 1 & 1 & 0 & 0\\ 0 & 0 & 0 & \sqrt{2} & -\sqrt{2} & 0\\ 0 & 1 & 0 & 0 & 1 & 1\end{bmatrix}^T \tag{44}$$

More detailed derivation and formulation of MITC3 may be found in (I. Katili et al., 2019). And so, the $\mathbf{B}^{\boldsymbol{\xi}}_{\mathbf{s\beta}_{\mathrm{MITC3}}}$ for generating stiffness matrix for shear can be obtained with,

$$\mathbf{B}^{\boldsymbol{\xi}}_{\mathbf{s\beta}_{\mathrm{MITC3}}} = \mathbf{B}^{\boldsymbol{\xi}}_{\mathbf{s\beta}_{\mathrm{T3\gamma}}} = \mathbf{N}_{\boldsymbol{\gamma}}\,\mathbf{A}_{\boldsymbol{\gamma}}\,\mathbf{A}_{\mathbf{u}} \tag{45}$$

$$\mathbf{N}_{\boldsymbol{\gamma}} = \boldsymbol{A}\,\boldsymbol{S} = \begin{bmatrix}A_1 + A_2 & -\sqrt{2}\,A_3 & A_3\\ A_2 & \sqrt{2}\,A_2 & A_1 + A_3\end{bmatrix} \tag{46}$$

$$\mathbf{A}_{\boldsymbol{\gamma}} = \begin{bmatrix}L_4 & 0 & 0\\ 0 & \frac{L_5}{\sqrt{2}} & 0\\ 0 & 0 & -L_6\end{bmatrix} \tag{47}$$

$$\mathbf{A}_{\mathbf{u}} = \frac{1}{2}\begin{bmatrix}-\frac{2}{L_4} & C_4 & S_4 & \frac{2}{L_4} & C_4 & S_4 & 0 & 0 & 0\\ 0 & 0 & 0 & -\frac{2}{L_5} & C_5 & S_5 & \frac{2}{L_5} & C_5 & S_5\\ \frac{2}{L_6} & C_6 & S_6 & 0 & 0 & 0 & -\frac{2}{L_6} & C_6 & S_6\end{bmatrix} \tag{48}$$

where C_k and S_k are the direction cosines of side *i-j* (Figure 3). It is at this stage that the KI becomes difficult to apply due to the formation of the MITC3 shear curvature which requires the relationship only between *nodes* inside the element.

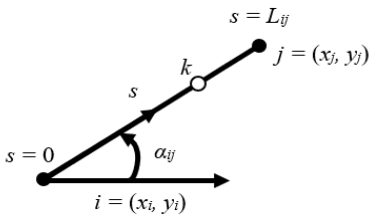

$C_k = C_{ij} = cos\ \alpha_{ij} = x_{ji}/L_{ij}$

$S_k = S_{ij} = sin\ \alpha_{ij} = y_{ji}/L_{ij}$

$L_k^2 = L_{ij}^2 = x_{ij}^2 + y_{ji}^2$

Figure 3. The Direction Cosines of Side *i-j*
Source: (I. Katili et al., 2019)

The new TS matrix for completing $\mathbf{B}^{\boldsymbol{\xi}}_{\mathbf{s\beta}_{\mathrm{MITC3+}}}$ matrix is described as follows,

$$\mathbf{B}^{\boldsymbol{\xi}}_{\mathbf{s\beta}_+} = -\hat{d}\left[\mathbf{B}^{\mathbf{1\xi}}_{\mathbf{s\beta}_+}\ \mathbf{B}^{\mathbf{2\xi}}_{\mathbf{s\beta}_+}\ \mathbf{B}^{\mathbf{3\xi}}_{\mathbf{s\beta}_+}\right] \tag{49}$$

$$\mathbf{B}^{\mathbf{1\xi}}_{\mathbf{s\beta}_+} = \begin{bmatrix}0 & x_{32}(3\eta - 1) & y_{32}(3\eta - 1)\\ 0 & x_{32}(1 - 3\xi) & y_{32}(1 - 3\xi)\end{bmatrix} \tag{50}$$

$$\mathbf{B}^{\mathbf{2\xi}}_{\mathbf{s\beta}_+} = \begin{bmatrix}0 & x_{13}(3\eta - 1) & y_{13}(3\eta - 1)\\ 0 & x_{13}(1 - 3\xi) & y_{13}(1 - 3\xi)\end{bmatrix} \tag{51}$$

$$\mathbf{B}^{\mathbf{3\xi}}_{\mathbf{s\beta}_+} = \begin{bmatrix}0 & x_{21}(3\eta - 1) & y_{21}(3\eta - 1)\\ 0 & x_{21}(1 - 3\xi) & y_{21}(1 - 3\xi)\end{bmatrix} \tag{52}$$

with $x_{32} = x_3 - x_2$ and $y_{32} = y_3 - y_2$. The x_i and y_i are the coordinates of node *i* on the corner of the element concerning the Cartesian coordinate system. The value of $\hat{d} = \frac{1}{6} - p$ with $p = 10^{-4}$, so the value of $\hat{d}$ is very close to 1/6 (I. Katili et al., 2019). The last components of the shear stiffness matrix are the additional TS field for the additional rotational *dof*,

$$\mathbf{B}^{\boldsymbol{\xi}}_{\mathbf{s\Delta\beta_{MITC3+}}} = \frac{1}{2}\begin{bmatrix} x_{21} & y_{21} \\ -x_{13} & -y_{13} \end{bmatrix} \tag{53}$$

The final form of shear curvatures can get in the Cartesian coordinate system by incorporating previous Jacobian matrix,

$$\boldsymbol{\gamma} = \begin{Bmatrix} \gamma_x \\ \gamma_y \end{Bmatrix} = \mathbf{j}\begin{Bmatrix} \gamma_\xi \\ \gamma_\eta \end{Bmatrix} = \mathbf{j}\,\mathbf{B}^{\boldsymbol{\xi}}_{\mathbf{s\beta}_{\mathrm{MITC3+}}}\mathbf{d} + \mathbf{j}\,\mathbf{B}^{\boldsymbol{\xi}}_{\mathbf{s\Delta\beta}_{\mathrm{MITC3+}}}\boldsymbol{\Delta\beta_\eta} \tag{54}$$

From this stage, the stiffness matrix of the Kriging-based MITC3+ needs to be condensed first to obtain 9 *dof* element. The static condensation starts by expressing the total strain energy of the element which is divided by bending energy U_b and shear energy U_s. The bending energy for one element of the Kriging-based MITC3+ can be expressed as,

$$U_b = \frac{1}{2}\int_A \boldsymbol{\kappa}\, D_b\, \boldsymbol{\kappa}\, dA \tag{55}$$

and in matrix form, it can be written as,

$$U_b = \frac{1}{2}\begin{Bmatrix} \mathbf{d} \\ \Delta\boldsymbol{\beta}_\mathbf{n} \end{Bmatrix}^{\mathrm{T}}\begin{bmatrix} \mathbf{k_{b11}} & \mathbf{k_{b12}} \\ \mathbf{k_{b21}} & \mathbf{k_{b22}} \end{bmatrix}\begin{Bmatrix} \mathbf{d} \\ \Delta\boldsymbol{\beta}_\mathbf{n} \end{Bmatrix} \tag{56}$$

The stiffness components that will be used for the static condensation from the bending stiffness matrix is,

$$\mathbf{k_{b11}} = \int_A \mathbf{B_{b\beta}}^{\mathbf{T}} D_b\, \mathbf{B_{b\beta}}\, dA \tag{57}$$

$$\mathbf{k_{b22}} = \int_A \mathbf{B_{b\Delta\beta}}^{\mathrm{T}} D_b\, \mathbf{B_{b\Delta\beta}}\, dA \tag{58}$$

And for the *shear strain energy* for one element can be expressed as,

$$U_s = \frac{1}{2}\int_A \boldsymbol{\gamma}^* D_s \boldsymbol{\gamma}^*\, dA \tag{59}$$

and in matrix form, it can be written as,

$$U_s = \frac{1}{2}\begin{Bmatrix} \mathbf{d} \\ \Delta\boldsymbol{\beta}_\mathbf{n} \end{Bmatrix}^{\mathrm{T}}\begin{bmatrix} \mathbf{k_{s11}} & \mathbf{k_{s12}} \\ \mathbf{k_{s21}} & \mathbf{k_{s22}} \end{bmatrix}\begin{Bmatrix} \mathbf{d} \\ \Delta\boldsymbol{\beta}_\mathbf{n} \end{Bmatrix} \tag{60}$$

And for the stiffness components that will be used for the condensation is,

$$\mathbf{k_{s11}} = \int_A \mathbf{B_{s\beta}}^{\mathrm{T}}_{\mathrm{MITC3+}} D_s\, \mathbf{B_{s\beta}}_{\mathrm{MITC3+}}\, dA \tag{61}$$

$$\mathbf{k_{s22}} = \int_A \mathbf{B_{s\Delta\beta}}^{\mathrm{T}}_{\mathrm{MITC3+}} D_s\, \mathbf{B_{s\Delta\beta}}_{\mathrm{MITC3+}}\, dA \tag{62}$$

$$\mathbf{k_{s12}} = \int_A \mathbf{B_{s\beta}}_{\mathrm{MITC3+}}^{\mathrm{T}} D_s \, \mathbf{B_{s\Delta\beta}}_{\mathrm{MITC3+}} dA \;;\; \mathbf{k_{s12}} = \mathbf{k_{s21}}^T \tag{63}$$

The equation for the *total strain energy* in the *principle of potential energy* now can be written as,

$$U = U_b + U_s + U_{external} \tag{64}$$

$$U = \frac{1}{2}\begin{Bmatrix} \mathbf{d} \\ \Delta\boldsymbol{\beta}_\mathbf{n} \end{Bmatrix}^{\mathrm{T}} \begin{bmatrix} \mathbf{k_{11}} & \mathbf{k_{12}} \\ \mathbf{k_{21}} & \mathbf{k_{22}} \end{bmatrix} \begin{Bmatrix} \mathbf{d} \\ \Delta\boldsymbol{\beta}_\mathbf{n} \end{Bmatrix} - \begin{Bmatrix} \mathbf{d} \\ \Delta\boldsymbol{\beta}_\mathbf{n} \end{Bmatrix}^{T} \begin{Bmatrix} \mathbf{f_n} \\ \mathbf{0} \end{Bmatrix} \tag{65}$$

$$\mathbf{k_{11}} = \mathbf{k_{b11}} + \mathbf{k_{s11}} \tag{66}$$

$$\mathbf{k_{12}} = \mathbf{k_{s12}} \tag{67}$$

$$\mathbf{k_{21}} = \mathbf{k_{s21}} \tag{68}$$

$$\mathbf{k_{22}} = \mathbf{k_{b22}} + \mathbf{k_{s22}} \tag{69}$$

The $\boldsymbol{k_b}$ and $\boldsymbol{k_s}$ matrix are stiffness matrix that are formed when an element still has an additional *bubble function* in the middle of the element. Therefore, the variation of the total energy (*U*) to the existence of the internal *bubble function* variable ($\Delta\boldsymbol{\beta}_\mathbf{n}$) requires the condition of,

$$\mathbf{k_{21}}\,\mathbf{d} + \mathbf{k_{22}}\,\Delta\boldsymbol{\beta}_\mathbf{n} = 0 \tag{70}$$

So the condensation component **Au** obtain as,

$$\Delta\boldsymbol{\beta}_\mathbf{n} = \mathbf{Au}\,\mathbf{d} \tag{71}$$

$$\mathbf{Au} = -\mathbf{k_{22}}^{-1}\mathbf{k_{21}} \tag{72}$$

The final bending and shear curvature for generating stiffness matrix can be obtain by using this equation,

$$\boldsymbol{\kappa} = \mathbf{B_{b_{MITC3+}}}\,\mathbf{d} \tag{73}$$

$$\mathbf{B_{b_{MITC3+}}} = \mathbf{B_{b\beta_{MITC3+}}} - \mathbf{B_{b\Delta\beta_{MITC3+}}}\mathbf{k_{22}}^{-1}\mathbf{k_{21}} \tag{74}$$

$$\boldsymbol{\gamma} = \mathbf{B_{s_{MITC3+}}}\,\mathbf{d} \tag{75}$$

$$\mathbf{B_{s_{MITC3+}}} = \mathbf{B_{s\beta_{MITC3+}}} - \mathbf{B_{s\Delta\beta_{MITC3+}}}\mathbf{k_{22}}^{-1}\mathbf{k_{21}} \tag{76}$$

The internal force of moment **M** and shear **Q** can be obtain using stress-strain law as follows,

$$\mathbf{M} = \frac{t^3}{12}\mathbf{E}_\mathrm{b}\boldsymbol{\kappa} = \mathbf{D}_\mathrm{b}\boldsymbol{\kappa} \tag{77}$$

$$\mathbf{Q} = k\,t\,\mathbf{E}_\mathrm{s}\boldsymbol{\varepsilon}_\mathrm{s} = \mathbf{D}_\mathrm{s}\boldsymbol{\varepsilon}_\mathrm{s} \tag{78}$$

As for the *Global discretized* equilibrium equation, it can be obtained from the element equilibrium equation with the assembly procedure using the *direct stiffness method* conceptual. It should be mentioned that the assembly process of each element also includes all *nodes* in the element of DOI. After that, the global equilibrium equation can be obtained as;

$$\mathbf{KD} = \mathbf{F} \tag{79}$$

With **K** is the global stiffness matrix, **D** is the global nodal displacement, and **F** is the global nodal load vector.

4. NUMERICAL TEST

This chapter will focus on the performance results of the MITC3+ element in solving various numerical problems. The results obtained will then be compared with the exact solution from the reference and also compared with the solution obtained from the results of previous paper research (Wijaya, 2016). The results from the previous research (Wijaya, 2016) were obtained using the discrete shear gap (DSG) method to overcome the shear-locking problem in the triangular K-FEM element. This test is carried out to see the behavior arising from the formulation of MITC3+ elements based on the Kriging interpolation. Hence a *Patch Test* is carried out and then followed by shear-locking test, convergence test, and plotting the internal force obtained and using it for the comparison with the exact value.
The *Patch Test* conducted in this study is to test the ability of an element to produce a state of constant strain or stress that it supposed to. Testing is done by comparing the accuracy of the MITC3+ with the reference solution. The *Patch Test* is carried out in two conditions, namely the constant curvature and the constant shear strain test. Furthermore, the test was continued to see the convergence ability of the elements when the mesh was smoothed with the same plate shape.

4.1. Constant Curvature Patch Test

Consider a hard clamped plate with the dimension as in Figure 4, with the coordinates of the *nodes* for the formation of the mesh shown in Table 4.1. The load given to the plate is in the form of prescribed displacement on the four sides of the rectangle. The material properties to be used are $E = 1.0 \times 10^6$ and $v = 0.25$, while for the thickness of the plate, the value of $h = 0.001$ is taken so that the length-to-thickness ratio $(L/h) = 240$.

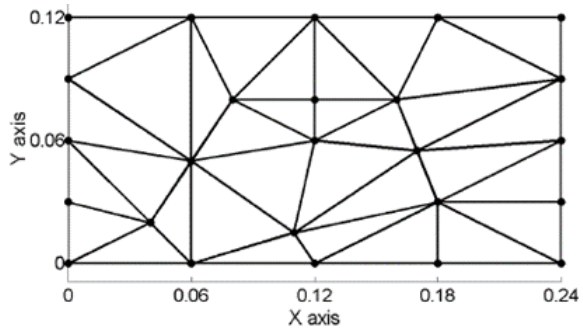

Figure 4. *Patch Test* Element Mesh with 25 *Nodes*
Source: (Wong & Kanok-Nukulchai, 2009)

Table 2. Location of Node on *Patch Test*

Node	Coordinate		Node	Coordinate		Node	Coordinate		Node	Coordinate		Node	Coordinate	
	x	y		x	y		x	y		x	y		x	y
1	0	0	6	0	0.03	11	0	0.06	16	0	0.09	21	0	0.12
2	0.06	0	7	0.04	0.02	12	0.06	0.05	17	0.08	0.08	22	0.06	0.12
3	0.12	0	8	0.11	0.015	13	0.12	0.06	18	0.12	0.08	23	0.12	0.12
4	0.18	0	9	0.18	0.03	14	0.17	0.055	19	0.16	0.08	24	0.18	0.12
5	0.24	0	10	0.24	0.03	15	0.24	0.06	20	0.24	0.09	25	0.24	0.12

The prescribed displacement loads given to the plate are:

$w = 10^{-3} (x^2 + xy + y^2) / 2$ (80)
$\beta_x = 10^{-3} (x / 2 + y)$ (81)
$\beta_y = 10^{-3} (- x - y / 2)$ (82)

This load will result in constant curvature and bending moments of

$$\boldsymbol{\kappa} = \begin{Bmatrix} 1 \\ 1 \\ 1 \end{Bmatrix} \times 10^{-3}, \qquad \mathbf{M} = -\begin{Bmatrix} 10/9 \\ 10/9 \\ 1/3 \end{Bmatrix} \times 10^{-7} \tag{83}$$

Comparisons are made by looking at the results of the calculation of the maximum relative error for the nodal displacement and nodal moment. The definition of relative error is as follows,

$e = | (w_{app} - w_{exact}) / w_{exact} |$ (84)

where w_{app} is the value of approximation obtained, w_{exact} is the exact solution value.
The results of the calculation of the maximum relative error for nodal displacement, moment, and shear force can be seen in Table 3, Table 4, and Table 5. From there it appears that the MITC3 + element on the P1-QS-1 (linear polynomial, quartic spline, one layer) has given good results with an order of error -13 to -17. However, when using P2-QS-2 and P3-QS-3, the relative error order of MITC3+ jumped very high to be greater than the results of previous studies using DSG. With these bad results, it can be said that MITC3+ still does not pass this *Patch Test*.

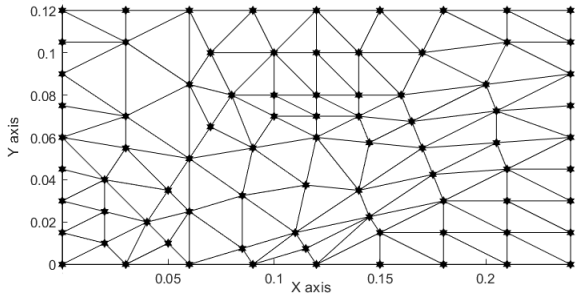

Figure 5. *Patch Test* Element Mesh with 81 *Nodes*

The convergence test on the *Patch Test* plate was finally carried out to see the shape of the convergence pattern when the mesh is smoothed as shown in Figure 5. The results of this test show that the convergence pattern of MITC3 + worsens, especially errors at the nodal moment and displacement. However, by changing the Kriging layer parameter to 2 levels above the polynomial level, you can get better results than before. Therefore, the poor results in this one case still need further investigation.

Table 3. Nodal Displacements Maximum Relative Error for *Constant Curvature Patch Test*

K-FEM Option	K-FEM			DSG			MITC3+ (25 *Nodes*)		
	P1-QS-1	P2-QS-2	P3-QS-3	P1-QS-1	P2-QS-2	P3-QS-3	P1-QS-1	P2-QS-2	P3-QS-3
w	9.26E-02	5.13E-05	4.04E-05	2.23E-14	8.88E-04	2.98E-04	7.90E-15	2.80E-02	9.60E-03
θx	1.26E-01	1.63E-04	6.77E-05	8.89E-14	6.38E-03	4.31E-03	6.20E-14	1.30E-01	5.70E-02
θy	1.31E-01	1.53E-04	7.74E-05	8.64E-14	2.26E-03	6.52E-04	3.40E-14	7.40E-02	4.30E-02
Max Error	1.31E-01	1.63E-04	7.74E-05	8.89E-14	6.38E-03	4.31E-03	6.20E-14	1.30E-01	5.70E-02

Table 4. Nodal Moments Maximum Relative Error for *Constant Curvature Patch Test*

K-FEM Option	K-FEM			DSG			MITC3+ (25 *Nodes*)		
	P1-QS-1	P2-QS-2	P3-QS-3	P1-QS-1	P2-QS-2	P3-QS-3	P1-QS-1	P2-QS-2	P3-QS-3
Mx	1.99E-01	4.69E-04	2.92E-04	1.88E-13	5.48E-03	2.72E-03	3.50E-14	1.89E-01	1.33E-01
My	2.98E-01	6.65E-04	4.61E-04	3.08E-13	1.20E-02	5.92E-03	7.30E-14	6.76E-01	1.68E-01
Mxy	2.76E-01	3.70E-04	3.01E-04	3.98E-13	7.92E-03	5.18E-03	1.70E-13	1.61E-01	2.38E-01
Max Error	2.98E-01	6.65E-04	4.61E-04	3.98E-13	1.20E-02	5.92E-03	1.70E-13	6.76E-01	2.38E-01

Table 5. Maximum Shear Forces for *Constant Curvature Patch Test*

K-FEM Option	K-FEM			DSG			MITC3+ (25 *Nodes*)		
	P1-QS-1	P2-QS-2	P3-QS-3	P1-QS-1	P2-QS-2	P3-QS-3	P1-QS-1	P2-QS-2	P3-QS-3
Qx	1.09E-02	2.10E-06	1.13E-06	2.23E-16	1.30E-05	3.42E-06	5.39E-17	4.00E-06	2.06E-06
Qy	6.99E-03	1.84E-06	1.65E-06	2.42E-16	8.39E-06	3.53E-06	2.48E-16	3.75E-06	2.05E-06
Max Error	1.09E-02	2.10E-06	1.65E-06	2.42E-16	1.30E-05	3.53E-06	2.48E-16	4.00E-06	2.06E-06

4.2. Constants Shear Patch Test

The same plate with the same property from the previous test is used in the *constant shear Patch Test*. But, for thickness of the plate used in this test is taken so the *L/h* = 0,024 (*h* = 10) and second *L/h* = 0.0024 (*h* = 100). The prescribed displacement loads given to the side of the plate are,

$$w = 10^{-6} (x + y) / 2 \quad (85)$$

$$\theta_x = \psi_y = -1/2 \times 10^{-6} \quad (86)$$

$$\theta_y = -\psi_x = 1/2 \times 10^{-6} \quad (87)$$

This condition should give a shear dominant result of,

$$\boldsymbol{\varepsilon}_s = \{1 \quad 1\}^{\mathrm{T}} \times 10^{-6}, \qquad \boldsymbol{\kappa} \cong \{0 \quad 0 \quad 0\}^{\mathrm{T}} \tag{88}$$

$$\mathbf{Q} = \{10/3 \quad 10/3\}^{\mathrm{T}}\ , \quad \text{for } L/h = 0{,}024 \tag{89}$$

$$\mathbf{Q} = \{100/3 \quad 100/3\}^{\mathrm{T}}\ , \quad \text{for } L/h = 0{,}0024 \tag{90}$$

The result from the *constant shear patch test* is shown on Table 6 and Table 7. Comparisons are made by looking at the results of the calculation of the maximum relative error for nodal displacement and shear force. Different from the previous *Patch Test*, not only MITC3+ on P1-QS-1 that give a better result than DSG element, but also on P2-QS-2 and P3-QS-3. Even so, the MITC3+ still not pass this test, because the resulting error order level is still between -4 to -7. However, upon further investigation of the convergence, the MITC3+ in this constant shear condition was able to produce a convergence pattern that improves as the mesh is smoothed like Figure 5.

Table 6. *Maximum Relative Error* for *Constant Shear Patch Test* with *L/h* = 0.024

K-FEM Options	K-FEM			DSG			MITC3+ (25 *Nodes*)		
	P1-QS-1	P2-QS-2	P3-QS-3	P1-QS-1	P2-QS-2	P3-QS-3	P1-QS-1	P2-QS-2	P3-QS-3
w	2.03.E-05	9.42.E-02	4.62.E-02	3.47.E-05	5.86.E-05	3.41.E-05	2.60.E-05	5.12.E-05	3.10.E-05
θx	1.32.E-04	1.62.E-04	1.40.E-04	1.84.E-04	3.40.E-04	1.81.E-04	1.32.E-04	2.76.E-04	1.87.E-04
θy	2.43.E-04	2.59.E-04	2.34.E-04	2.53.E-04	5.70.E-04	2.86.E-04	2.43.E-04	5.32.E-04	3.14.E-04
Qx	1.09.E-04	2.36.E-01	7.45.E-02	9.91.E-05	1.82.E-04	1.04.E-04	9.58.E-05	1.70.E-04	1.13.E-04
Qy	6.42.E-05	1.18.E-01	9.85.E-02	6.39.E-05	1.12.E-04	6.87.E-05	6.02.E-05	1.02.E-04	7.65.E-05

Table 7. *Maximum Relative Error* for *Constant Shear Patch Test* with *L/h* = 0.0024

K-FEM Options	K-FEM			DSG			MITC3+ (25 *Nodes*)		
	P1-QS-1	P2-QS-2	P3-QS-3	P1-QS-1	P2-QS-2	P3-QS-3	P1-QS-1	P2-QS-2	P3-QS-3
w	2.03.E-07	9.42.E-02	4.62.E-02	3.47.E-07	5.86.E-07	3.42.E-07	2.60.E-07	5.12.E-07	3.10.E-07
θx	1.32.E-06	1.62.E-06	1.40.E-06	1.84.E-06	3.41.E-06	1.81.E-06	1.32.E-06	2.76.E-06	1.87.E-06
θy	2.43.E-06	2.59.E-06	2.34.E-06	2.53.E-06	5.70.E-06	2.86.E-06	2.43.E-06	5.32.E-06	3.14.E-06
Qx	1.09.E-06	2.36.E-01	7.44.E-02	9.91.E-07	1.82.E-06	1.04.E-06	9.58.E-07	1.70.E-06	1.13.E-06
Qy	6.42.E-07	1.18.E-01	9.85.E-02	6.40.E-07	1.12.E-06	6.87.E-07	6.02.E-07	1.02.E-06	7.65.E-07

4.3. Shear Locking Test

A square plate with hard clamped support on the perimeter were used for the shear-locking test. The plate and mesh configuration can be seen in Figure 6. The result show that with every polynomial basis, the MITC3+ was able to avoid the shear-locking mechanism completely until *L/h* = 100.000. Its performance was also appears better than the previous research (Wijaya, 2016) using DSG method, where the shear-locking already start to appear on *L/h* = 1000.

Consider the square plate with the dimension of 100 × 100 under uniform loading of $f_z = 1$ is used for the *shear locking* test. Because of symmetry, only a quarter of the plate is considered with hard clamped support condition along two sides and the symmetry condition of $\beta_x = 0$ along one other side and $\beta_y = 0$ on the last one side. The configuration of the mesh can be seen in Figure 6. The material properties used are $E = 2.0 \times 10^6$ and $v = 0.3$. The test was carried out to look for the value of the center deflection in plate with several variations the plate

thickness, namely *L/h* = 5, 10, 100, 1,000, 10.000, and 100.000. The result for the normalized center displacement of the square plate shown in Table 8.

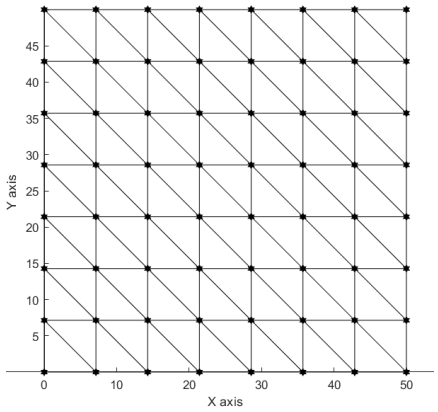

Figure 6. Square Plate Dimension and Mesh Configuration

Table 8. The Rectangular Plate Normalized Center Deflection Value

(a) P1-QS-1

L/h	5	10	100	1000	10000	100000
K-FEM	1.604	0.983	0.056	0.001	0.000	0.000
DSG	1.673	1.149	0.862	0.362	0.310	0.310
MITC3+	1.671	1.152	0.966	0.963	0.963	0.942
Exact Solution	1.000	1.000	1.000	1.000	1.000	1.000

(b) P2-QS-2

L/h	5	10	100	1000	10000	100000
K-FEM	1.718	1.191	0.878	0.081	0.000	0.000
DSG	1.735	1.209	1.003	0.885	0.21	0.003
MITC3+	1.673	1.146	0.950	0.947	0.947	0.926
Exact Solution	1.000	1.000	1.000	1.000	1.000	1.000

(c) P3-QS-3

L/h	5	10	100	1000	10000	100000
K-FEM	1.720	1.191	0.992	0.613	0.015	0.000
DSG	1.735	1.209	1.008	0.992	0.675	0.021
MITC3+	1.676	1.147	0.946	0.943	0.943	0.922
Exact Solution	1.000	1.000	1.000	1.000	1.000	1.000

4.4. Rhombic Plate

A *Rhombic Plate* with a size of *L* = 100 m with an angle of 30^0 (critical angle) was used for the element convergence test as the plate thin out, this was done because many elements failed on the rhombic plate at this critical angle. The plate has joint support on each side. Testing was carried out on two variations of plate thickness, namely *L/h* = 100 and 1000. The dimensions and material properties of the plates can be seen in Figure 7.

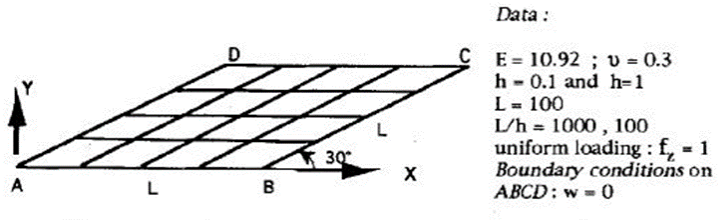

Figure 7. Dimension and Material Property of the Rhombic Plate
Source: (I. Katili, 1993)

Furthermore, the plate will be divided into several mesh models, namely 4 × 4, 8 × 8, 16 × 16, and 32 × 32 elements. The mesh shape of the plate can be seen in Figure 8.

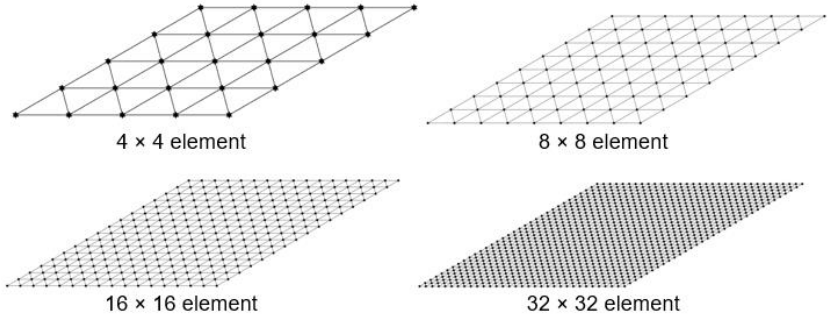

Figure 8. Mesh Configuration of the Rhombic Plate

The test was done by looking for the center deflection values, maximum and minimum moments (principal moments) that occur at the center of the plate. The normalization of the obtained result against the exact solution from reference will be compared to see the convergence pattern while the number of element being increase like shown in Figure 8. The results of the convergence of the center deflection, maximum and minimum moments for each polynomial basis of K-FEM option and thickness are shown from Table 9 to Table 15.
The MITC3+ is able to get more accurate solution as the number of elements is multiplied which means the element are able to converge unlike the previous convergence test on the *constant curvature patch test*.

Table 9. Convergence of Center Deflection Value of Rhombic Plate (*L/h=100*)

(a) P1-QS-1

Mesh	4	8	16	32
K-FEM	0.024	0.086	0.266	0.577
DSG	0.890	0.928	0.988	1.020
MITC3+	0.965	1.009	1.022	1.028
Exact Solution	1.000	1.000	1.000	1.000

(b) P2-QS-2

Mesh	4	8	16	32
K-FEM	0.232	0.694	0.966	1.022
DSG	0.943	0.927	0.984	1.017
MITC3+	1.002	1.003	1.016	1.024
Exact Solution	1.000	1.000	1.000	1.000

(c) P3-QS-3

Mesh	4	8	16	32
K-FEM	0.381	0.869	0.996	1.027
DSG	0.848	0.907	0.977	1.014
MITC3+	0.925	0.986	1.009	1.021
Exact Solution	1.000	1.000	1.000	1.000

Table 10. Convergence of Maximum Moment Value of Rhombic Plate (*L/h=100*)

(a) P1-QS-1

Mesh	4	8	16	32
K-FEM	0.021	0.086	0.272	0.583
DSG	0.817	0.962	0.998	1.009
MITC3+	0.847	0.977	1.004	1.013
Exact Solution	1.000	1.000	1.000	1.000

(b) P2-QS-2

Mesh	4	8	16	32
K-FEM	0.143	0.755	0.971	1.010
DSG	0.911	0.988	1.004	1.009
MITC3+	0.943	0.999	1.007	1.013
Exact Solution	1.000	1.000	1.000	1.000

(c) P3-QS-3

Mesh	4	8	16	32
K-FEM	0.301	0.892	0.993	1.015
DSG	0.854	0.994	1.004	1.007
MITC3+	0.888	0.997	1.005	1.011
Exact Solution	1.000	1.000	1.000	1.000

Table 11. Convergence of Minimum Moment Value of Rhombic Plate (*L/h=100*)

(a) P1-QS-1

Mesh	4	8	16	32
K-FEM	0.017	0.075	0.244	0.550
DSG	0.852	1.066	1.081	1.036
MITC3+	0.827	0.994	1.024	1.038
Exact Solution	1.000	1.000	1.000	1.000

(b) P2-QS-2

Mesh	4	8	16	32
K-FEM	0.118	0.629	0.934	1.029
DSG	1.005	1.129	1.100	1.035
MITC3+	0.957	1.041	1.033	1.037
Exact Solution	1.000	1.000	1.000	1.000

(c) P3-QS-3

Mesh	4	8	16	32
K-FEM	0.270	0.818	0.994	1.039
DSG	1.068	1.194	1.111	1.033
MITC3+	0.998	1.069	1.034	1.035
Exact Solution	1.000	1.000	1.000	1.000

Table 12. Convergence of Center Deflection Value of Rhombic Plate (*L/h=1000*)

(a) P1-QS-1

Mesh	4	8	16	32
K-FEM	0.000	0.001	0.004	0.015
DSG	0.885	0.755	0.761	0.849
MITC3+	0.963	1.005	1.013	1.013
Exact Solution	1.000	1.000	1.000	1.000

(b) P2-QS-2

Mesh	4	8	16	32
K-FEM	0.004	0.031	0.254	0.699
DSG	0.935	0.747	0.755	0.844
MITC3+	1.000	1.000	1.009	1.010
Exact Solution	1.000	1.000	1.000	1.000

(c) P3-QS-3

Mesh	4	8	16	32
K-FEM	0.010	0.169	0.644	0.829
DSG	0.716	0.716	0.747	0.841
MITC3+	0.923	0.983	1.003	1.007
Exact Solution	1.000	1.000	1.000	1.000

Table 13. Convergence of Maximum Moment Value of Rhombic Plate (*L/h=1000*)

(a) P1-QS-1

Mesh	4	8	16	32
K-FEM	0.000	0.001	0.004	0.016
DSG	0.817	0.821	0.894	0.966
MITC3+	0.846	0.977	1.000	1.005
Exact Solution	1.000	1.000	1.000	1.000

(b) P2-QS-2

Mesh	4	8	16	32
K-FEM	0.002	0.031	0.331	0.804
DSG	0.909	0.841	0.902	0.971
MITC3+	0.943	1.001	1.005	1.005
Exact Solution	1.000	1.000	1.000	1.000

(c) P3-QS-3

Mesh	4	8	16	32
K-FEM	0.007	0.207	0.808	0.893
DSG	0.859	0.845	0.913	0.979
MITC3+	0.889	1.000	1.003	1.003
Exact Solution	1.000	1.000	1.000	1.000

Table 14. Convergence of Minimum Moment Value of Rhombic Plate (*L/h=1000*)

(a) P1-QS-1

Mesh	4	8	16	32
K-FEM	0.000	0.001	0.003	0.014
DSG	0.869	1.020	1.135	1.247
MITC3+	0.827	0.995	1.018	1.021
Exact Solution	1.000	1.000	1.000	1.000

(b) P2-QS-2

Mesh	4	8	16	32
K-FEM	0.002	0.018	0.232	0.649
DSG	1.028	1.098	1.183	1.279
MITC3+	0.958	1.045	1.033	1.021
Exact Solution	1.000	1.000	1.000	1.000

(c) P3-QS-3

Mesh	4	8	16	32
K-FEM	0.005	0.110	0.646	0.771
DSG	1.114	1.202	1.265	1.334
MITC3+	1.000	1.076	1.036	1.019
Exact Solution	1.000	1.000	1.000	1.000

4.5. Complex-Shaped Plate

A rectangular plate with a heart-shaped hole was used to test the application of Kriging to MITC3 + elements in analyzing complex and free-form plates. The dimensions and mesh configuration of the plates can be seen in Figure 9. The test is carried out using hard clamped support on all four sides of the plate. The thickness (*h*) is taken 0.05 m, with the Modulus Young (*E*) = 200 x 10^9 N/m^2, Poisson' ratio = 0.3, and with the plate density ρ = 8000 kg/m3.

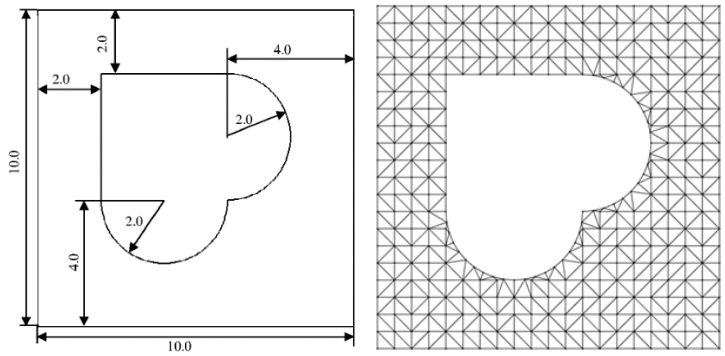

Figure 9. The Dimension and Material Properties of the Complex Plate

The maximum deflection and moment values are obtained and compared with the reference solution from the static DKMT element (Winata et al., 2016). The result of normalization of the values obtained against the reference solution are compared as shown in Table 15.
Overall, it appears that the MITC3+ with Kriging interpolation can provide accurate results and is very close to the reference solution like the DSG. This also happens even when the normalized maximum moment value obtained by DSG on P1-QS-1 shows a value of 0.740, while MITC3+ on P1-QS-1 can produce a value of 1.095 which is more accurate solution.

Table 15. Normalized Maximum Deflection and Maximum Moment

K-FEM Options		Max Deflection	Normalized Deflection	Max Moment	Normalized Moment
P1-QS-1	K-FEM	3.288E-04	0.025	1.279E+02	0.024
	MITC3+	1.327E-02	1.010	4.982E+03	1.095
	DSG	1.204E-02	0.902	3.997E+03	0.740
P2-QS-2	K-FEM	1.176E-02	0.881	4.747E+03	0.879
	MITC3+	1.313E-02	1.021	5.910E+03	0.923
	DSG	1.337E-02	1.002	5.651E+03	1.047
P3-QS-3	K-FEM	1.318E-02	0.987	5.689E+03	1.054
	MITC3+	1.316E-02	1.019	6.066E+03	0.899
	DSG	1.341E-02	1.005	5.804E+03	1.075
Reference Solution (Salim & Winata, 2016)		1.335E-02	1.000	5.399E+03	1.000

5. CONCLUDING REMARKS

The application and formulation of the MITC3+ on the Kriging-based finite element (K-FEM) has been successfully carried out in this study. MITC3+ showed satisfactory results and was able to do well in avoiding the shear-locking phenomenon that commonly occurs on thin plates. The accuracy of the Kriging-based MITC3+ element calculation has also been tested using complex-shaped plates, and it was found that MITC3+ was also able to produce accurate solutions that were close to the reference solution. Even so, further research still needs to be done regarding the convergence of the Kriging-based MITC3+ due to the large error and the tendency not to converge on the *constant curvature patch test*. Meanwhile on the *Rhombic Plate* convergence test, MITC3+ can provide a convergence pattern that is close to the solution of the DSG method and sometimes better. Research development can be done by trying to change the prescribed displacement on the *constant curvature patch test* with the prescribed moment along the 4 sides support of the plate. More advanced development can be done, namely by adding the Kriging interpolation scheme in constructing the shear stiffness matrix which in this research is only applied to the arrangement of bending stiffness matrix.

6. REFERENCES

Gu, L. (2003). Moving Kriging Interpolation and Element-free Galerkin Method. *International Journal for Numerical Methods in Engineering*, *56*(1), 1–11.

Jeon, H. M., Lee, Y., Lee, P. S., & Bathe, K. J. (2015). The MITC3+ Shell Element in Geometric Nonlinear Analysis. *Computers and Structures*, *146*, 91–104.

Katili, A. M., Maknun, I. J., & Katili, I. (2019a). Theoretical Equivalence and Numerical Performance of T3γ and MITC3 Plate Finite Elements. *Structural Engineering and Mechanics*, *69*(5), 527–536.

Katili, I. (1993). A New Discrete Kirchhoff-Mindlin Element Based on Mindlin-Reissner Plate Theory and Assumed Shear Strain Fields. *International Journal for Numerical Methods in Engineering*, *36*(August 1992), 1885–1908.

Katili, I., Jauhari Maknun, I., Batoz, J. L., & Katili, A. M. (2019). A Comparative Formulation of T3γ, DST, DKMT and MITC3+ Triangular Plate Elements with New Numerical Results Based on s-norm Tests. *European Journal of Mechanics*, 78.

Ko, Y., Lee, Y., Lee, P. S., & Bathe, K. J. (2017). Performance of The MITC3+ and MITC4+ Shell Elements in Widely-used Benchmark Problems. *Computers and Structures*, *193*, 187–206. http://dx.doi.org/10.1016/j.compstruc.2017.08.003

Lee, P. S., & Bathe, K. J. (2004). Development of MITC Isotropic Triangular Shell Finite Elements. *Computers and Structures*, *82*(11–12), 945–962.

Lee, P. S., Noh, H. C., & Bathe, K. J. (2007). Insight Into 3-node Triangular Shell Finite Elements: the Effects of Element Isotropy and Mesh Patterns. *Computers and Structures*, *85*(7–8), 404–418.

Lee, Y., Yoon, K., & Lee, P. S. (2012). Improving The MITC3 Shell Finite Element by Using The Hellinger-Reissner Principle. *Computers and Structures*, *110–111*, 93–106.

Nguyen-Xuan, H., Liu, G. R., Thai-Hoang, C., & Nguyen-Thoi, T. (2010). An Edge-Based Smoothed Finite Element Method (ES-FEM) With Stabilized Discrete Shear Gap Technique for Analysis of Reissner-Mindlin Plates. *Computer Methods in Applied Mechanics and Engineering*, *199*(9–12), 471–489. http://dx.doi.org/10.1016/j.cma.2009.09.001

Plengkhom, K., & Kanok-Nukulchai, W. (2005). An Enhancement of Finite Element Method With Moving Kriging Shape Functions. *International Journal of Computational Methods*, *02*(04), 451–475.

Tessler, A., & Hughes, T. J. R. (1985). A Three-node Mindlin Plate Element with Improved Transverse Shear. *Computer Methods in Applied Mechanics and Engineering*, *50*(1), 71–101.

Tongsuk, P., & Kanok-Nukulchai, W. (2004). Further Investigation of Element-Free Galerkin Method Using Moving Kriging Interpolation. *International Journal of Computational Methods*, *01*(02), 345–365.

Verwoerd, M. H., & Kok, A. W. M. (1990). A Shear Locking Free Six-node Mindlin Plate Bending Element. *Computers and Structures*, *36*(3), 547–551.

Wijaya, D. (2016). *Eliminasi Shear Locking pada Elemen Pelat Reissner-Mindlin Berbasis Kriging dengan Metode Discrete Shear Gap (DSG)*.

Winata, E. T., Salim, C. J., & Wong, F. T. (2016). *Studi Elemen Discrete-Kirchhoff Mindlin Triangle (DKMT) untuk Analisis Statik Pelat Lentur dan Pengembangan untuk Analisis Dinamik Getaran Bebas*.

Wong, F. T., & Kanok-Nukulchai, W. (2009). On the Convergence of the Kriging-based Finite Element Method. *International Journal of Computational Methods*, *6*(1), 93–118.

Wong, F. T., & Kanok-Nukulchai, W. (2006). On Alleviation of Shear Locking in the Kriging-Based Finite Element Method. *Proceedings of International Civil Engineering Conference "Towards Sustainable Engineering Practice," January*, 39–47.